OPEN ACCESS

University of BRISTOL

Krauskopf, B., Coetzee, E. B., & Lowenburg, M. H. (2011). Continuation analysis of aircraft ground loads during high-speed turns.

Early version, also known as pre-print

Link to publication record in Explore Bristol Research
PDF-document

University of Bristol - Explore Bristol Research

General rights

Continuation Analysis of Aircraft Ground Loads during High-speed Turns

Etienne Coetzee
Systems Engineering Specialist
Airbus Operations
Systems General
Bristol, UK, BS99 7AR
Email: etienne.coetzee@airbus.com

Bernd Krauskopf
Professor
Department of Engineering Mathematics
Faculty of Engineering
University of Bristol
Bristol, UK, BS8 1TR
Email: B.Krauskopf@bristol.ac.uk

Mark Lowenberg
Senior Lecturer
Department of Aerospace Engineering
Faculty of Engineering
University of Bristol
Bristol, UK, BS8 1TR
Email: M.Lowenberg@bristol.ac.uk

ABSTRACT

The current lateral ground loads requirement, FAR25.495, for an aircraft during a high-speed turn, was written in the middle of the last century, when relatively small aircraft with tricycle landing gear arrangements started to emerge. This requirement is known to be conservative when applied to large modern passenger aircraft. Nonlinearities (such as tyre forces) have a significant effect at the edge of operating envelopes, placing a renewed interest on analysis methods that can classify the dynamics in these regions. In this paper we use continuation methods to assess the loads that can be generated for different aircraft configurations during high-speed turns, and compare the results to the original requirement. A comparison is made between test results from an FAA study and continuation results, where all the significant test data points are located within an envelope constructed from continuation analysis. Continuation methods therefore provide a conservative estimate of the maximum lateral load factors. These values are however less than the value prescribed in the regulation.

1 Introduction

The aim of this study is to employ continuation methods to assess the loads that can be generated during typical operational ground manoeuvres for the Airbus A320 and A380. These results are compared with the current lateral ground loads requirement for an aircraft during a high-speed turn, FAR25.495, which was written in the middle of the last century, when relatively small aircraft with tricycle landing gear arrangements started to emerge. Modern aircraft are however quite different in terms of size and landing gear configuration, especially for an aircraft such as the A380. This requirement is known to be conservative for large aircraft such as the A380, where nonlinear effects, such as tyre forces, ensure that this aircraft does not experience the high lateral loads that are stipulated in the FAA requirement [1]. Comparisons are also made between the two aircraft types, which show significantly different dynamics in terms of stability and loads.

Section 2 discusses the limitations related to the requirement. It also discusses the main findings from an operational ground loads measurement campaign of in-service aircraft [2], which was specifically conducted to compare operational loads with
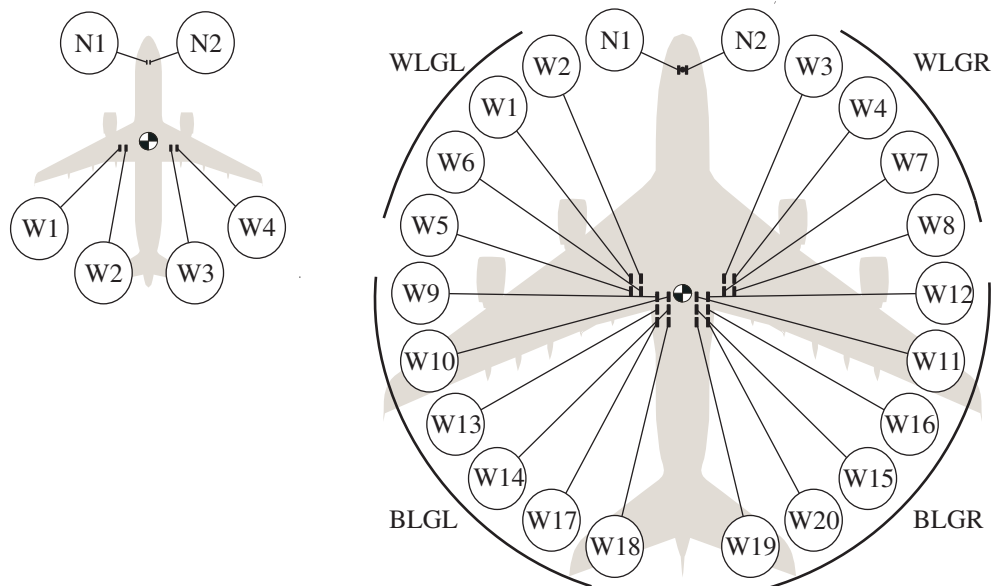
1

Figure 1: Wheel numbering definition for the A320 on the left, and the A380 on the right.

the requirement. This study confirmed that an increase in aircraft size is accompanied by a reduction in the maximum lateral load. A B747-400 experiences smaller lateral load factors compared to, say, an A320. The authors of [2] have also published some empirical formulae that were derived from the measured data, to help with predictions for aircraft that were not part of the study. These formulae are used here to make predictions of the maximum lateral loads that an aircraft such as the A380 is likely to experience in its lifetime.

In this study we use validated models of the A320 and the A380 [1, 3–5]. The A320 has three landing gears: one nose gear, and two main gears that are attached to the wings. Each gear has an axle with two wheels. The A380 has five landing gears: one nose gear, two main gears attached to the wings, and two main gears attached to the fuselage. Each wing landing gear (WLG) consists of a bogie with four wheels on each gear, while each body landing gear (BLG) consists of a bogie with six wheels. The aft axle of each BLG is steered. Six tyres are therefore present in the case of the A320 model, and 22 tyres in the A380 model. Figure 1 contains the numbering conventions of the wheels for both the A320 and A380 models.

The models that are used at Airbus are built with different test platforms in mind. MSC.Adams models are used for detailed ground manoeuvrability studies, while SimMechanics models are used on the test rigs, where the real-time performance of the models is critical. The MSC.Adams environment is user-friendly and is the preferred model development environment. MSC.Adams models are converted to SimMechanics for testing with the avionics that will be implemented on the aircraft. Figure 2 contains the SimMechanics representation of the A380. Similar models exist for the A320 and are used in exactly the same way. The high cost associated with simulations makes continuation techniques attractive, due to the speed with which a global picture of the dynamics can be constructed. Previous studies of the A320 showed how bifurcation methods can be used to detect stability margins, showing how specific bifurcations can be attributed to the loss of grip at specific tyres on the aircraft [1, 4, 5].

It is important to note that the simulation models that are used for the test rigs are in fact also used for the bifurcation analysis. This is a very useful feature, as these models are likely to be developed in other parts of the company. Hence it is possible to "plug" existing models into the bifurcation analysis framework provided by the Dynamical Systems Toolbox that was developed at the University of Bristol [3]. It allows for the seamless integration of Simulink or SimMechanics models, avoiding the rebuilding of models specifically for the purpose of bifurcation analysis. Another benefit of the toolbox is the additional information that can be obtained from the models. For instance, it is possible to represent the data in new ways that gives one a much better understanding of how the loads are distributed amongst the tyres. Figures 15 and 16 in Section 5.3 are a good example of new types of graphs that can be used to depict a global view of the force distribution in the tyres.

Section 3 compares dynamic and steady-state loads for an A320 and an A380 at a typical runway exit, and shows that the dynamic loads at the main gears are almost equal to the steady-state loads that are obtained from continuation methods. The load factor at the CG (for both aircraft) builds up towards a maximum value, without any overshoot. The maximum dynamic
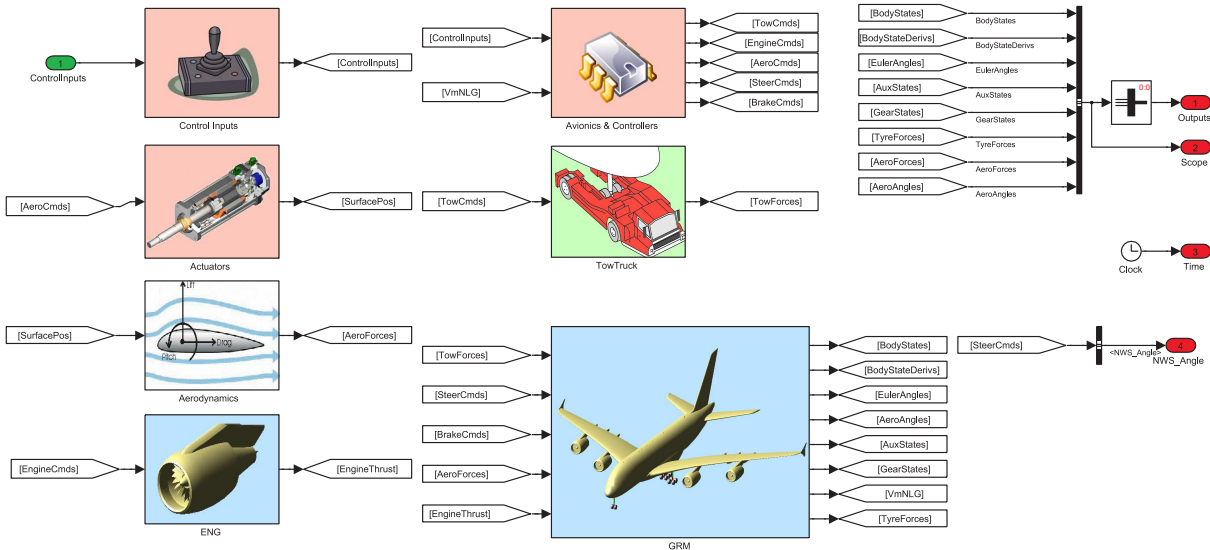
Figure 2: Top-level SimMechanics model of an A380.

tyre loads for the A320 are approximately 10% higher than the maximum steady-state values, while the steady-state tyre loads for most of the tyres of the A380 are in fact the maximum values. The dynamic values are 10% higher than the steady-state values on the aft axles of the BLGs. These findings are directly applicable to the high-speed turn that is discussed in this paper, where the regulation pertaining to the high-speed turn assumes steady-state conditions. We therefore propose that continuation methods can be used to obtain the loads at runway exits, and more significantly, the loads that are generated during high-speed turns. The use of continuation methods for lateral loads studies has previously been conducted on an aircraft with a traditional three post landing gear arrangement [6]. No lateral loads studies, using continuation methods, have so far been conducted on larger aircraft with more than three landing gears and multi-axle bogies.

Section 4 shows how aircraft manufacturers interpret the high-speed lateral loads requirement. A simple analysis method based on static balance equations is used to calculate accurate landing gear loads for an aircraft with three landing gears. This method can, however, not be employed for aircraft with more than two main gears (due to the static indeterminate nature of such landing gear arrangements). Multibody simulations are needed to obtain the dynamic response of the aircraft. Validated models and methods therefore form the basis of such predictions.

Section 5 contains the continuation results for the high-speed turn, as obtained from the detailed A320 and the A380 models. The analysis is conducted in accordance with the regulations at the maximum ramp weight (MRW) condition, with fore and aft CG positions. The stability results in Section 5.1 for the A320 compare well with the results from previous studies [1,4,5]. A clear boundary is formed by Hopf bifurcations, indicating a loss of grip at the inner main gear tyres [1, 4]. These areas of instability occur at relatively low speeds, hence the aerodynamics does not play any significant role as far as the A320 is concerned. The results in Section 5.2 for the A380 is significantly different from that of the A320: no bifurcations were detected, and the aircraft is in fact remarkably stable. Problematic areas are however identified in terms of manoeuvring at moderate velocities. The analysis shows that, when a runway exit turn is conducted, the nose gear tyres cannot generate enough side force above 8 m/s. The maximum prescribed velocity of 4 m/s for the A380 avoids this problem. We show that the gear loads can be classified across the entire operating envelope, where the WLGs act in the opposite direction to the BLGs at low velocities, contrary to the assumption in the regulation. Section 5.3 shows how continuation results can be used to assess the lateral load factors on individual tyres. Only the inner tyres in a turn experience load factors that are in the vicinity of the values stipulated by the requirement. The lateral load factors on the outer tyres are significantly less than the requirement, confirming its conservative nature.

Section 6 compares the maximum load values that were obtained from the operational loads measurement campaign with predicted results from continuation analysis. A maximum load factor envelope was constructed from the continuation results. All the significant data points are located within this envelope, showing that continuation methods provide a conservative estimate of the maximum lateral load factors. However, it is still less than the value prescribed in the regulation. This section also explains how an A320 could generate significant lateral loads. The velocity where this extreme value occurs is then used as an extreme case for the A380. The lateral load factor provided by continuation methods is approximately 10% larger than predicted from the operational study. Continuation methods do however provide complete coverage of the entire operating

3

envelope, allowing one to pinpoint the exact steering angle, and velocity, where the maximum load factor will occur.

2 Side Loads Requirements

One of the main design cases for aircraft ground loads pertains to the high-speed turn, which tends to be the critical case for the design of the attachments of the main landing gears. Federal Aviation Regulation (FAR) 25.495 [7] deals with this load case, and is phrased as follows:

> *"In the static position, in accordance with figure 7 [Figure 3(a)] of Appendix A, the aeroplane is assumed to execute a steady turn by nose gear steering, or by application of sufficient differential power, so that the limit load factors applied at the centre of gravity are 1.0 vertically and 0.5 laterally. The side ground reaction of each wheel must be 0.5 of the vertical reaction".*

Figure 3(a) depicts this requirement. The type of aircraft in the picture shows that the origins of the requirement are probably from the 1940's or 1950's. This load case forms one of the *bookcases* for ground loads as stated in the regulations [7], and needs to be considered by aircraft manufacturers in the design of their aircraft. All of these cases consist of static external forces that usually require ground reactions to be balanced by applying inertia forces and moments. We recap, by noting that the lateral load factor n_y is defined as the ratio of the lateral force over the vertical force, which is 0.5 for this specific regulation. Reference [2] states that little is known about the origin of this regulation, or even under what operational conditions such a loading condition might occur. The regulation was clearly brought in when aircraft were much smaller than they are nowadays, and it may be that aircraft with more than two main gears did not exist at the point in history when the regulation was drafted; however, we have no evidence for this assertion. Reference [2] also states that landing gear and aircraft manufacturers believe that the current 0.5g lateral load factor requirement specified by FAR 25.495 is too stringent. The regulatory authorities are however extremely reluctant to modify this requirement in the absence of data to back such a decision. The requirement has clearly ensured safe aircraft operations, and consequently overwhelming evidence would be needed for its relaxation.

2.1 Limitations of the Regulation

The loads produced by the high-speed turn form one of the limit load cases and, as such, contribute towards the aircraft and landing gear limit load envelopes. The loads can be calculated accurately for aircraft with statically determinate (tricycle) gear arrangements such as the A320, where the fuselage and gears are assumed to be rigid [4, 5]. However, statically indeterminate (more than three gears) arrangements such as the A380, pose computational challenges, where minimum energy techniques are needed to calculate the response of the aircraft [3]. Such an approach is needed to protect any one gear against disproportionate loading due to the stiffness characteristics of the gears and fuselage [8]. For this reason aircraft manufacturers tend to include other cases (in addition to the bookcases) into their analysis. These cases are based on years of experience that try to cover day-to-day operational scenarios. These additional cases are known as *rational* cases, as they utilise models that contain a more accurate representation of the real physics and dynamics of the system. In particular, the dynamic response of the airplane is included. Structural inertia, flexibility, and damping are accounted for, as well as distributed aerodynamic lift and moments. This is a more realistic method of investigating the actual forces on the aircraft.

Dynamic calculations are employed for rational cases such as taxiing or landing, and may form part of the limit load envelope. It is also normal practice to use such dynamic calculations to establish the aircraft fatigue loads. Nonlinear effects within the tyres and landing gears make it difficult to find the exact values for the steering angles and velocities where the maximum lateral loading may occur. This is the reason for adhering to the bookcase approach, with the addition of rational cases. Nonlinear effects could for instance lead to multiple steady-states for the same thrust and steering angle settings, when considering the high-speed turn, such that the response depends on the initial conditions and size of the perturbations on the system [1, 4]. A large perturbation could for instance cause a "jump" to another steady-state. This type of behaviour is the motivation to use methods from the field of Dynamical Systems theory, to analyse the dynamics of an aircraft on the ground [1, 3–6].

4
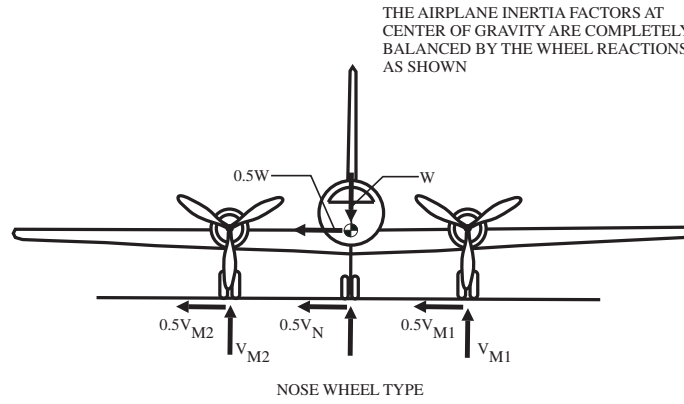
(a) Original image depicting the lateral load factor requirement; from [7].
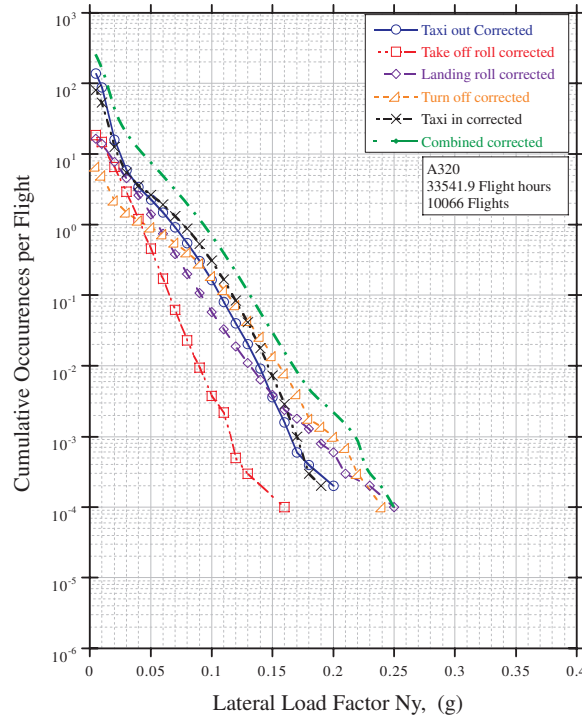
(b) Side loads as measured on an A320 aircraft; reproduced from [2].

Figure 3: FAR 25.495 side load requirements for the high-speed turn.

2.2 FAA Operational Loads Study

In answer to the points mentioned in the previous section and in Reference [2], the FAA conducted a large operational loads testing campaign, where it aimed to identify the maximum operational loads that can be experienced by in-service aircraft. A critical assessment of the loads was then made against the current regulations [2]. The findings from this study showed that it was very difficult to obtain lateral accelerations above 0.3g for any aircraft types. As an example, Figure 3(b) shows the measured side loads for the A320 that was used in [2]; it shows that they did not exceed 0.25g for the approximately 10,000 flights that were recorded. The authors of [2] collated the information for all the assessed aircraft and derived an empirical formula to predict the likelihood of obtaining a certain g-level in 1000 flights as

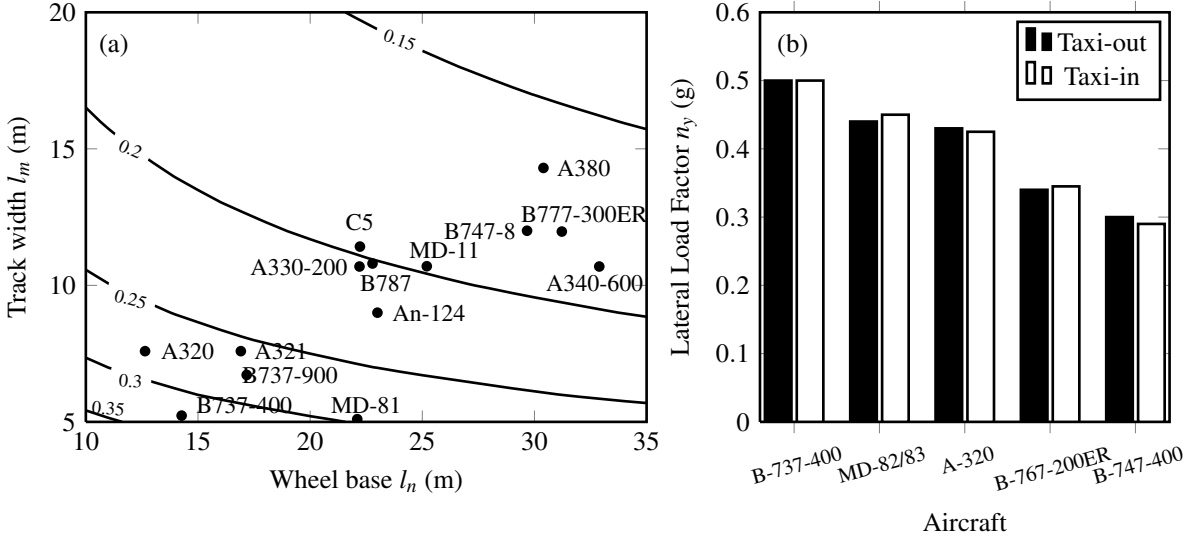$$N = N_0 e^{-l_n^s l_m n_y^2}. \tag{1}$$

5

Figure 4: Predicted lateral load factors obtained from FAA operational loads study [2]. The contours in panel (a) represent the maximum load that can be expected at least once in 100,000 flights, while panel (b) compares the equal probability lateral load factors during ground turning for five aircraft; reproduced from [2].

Here N is the number of cumulative occurrences of any lateral load factor n_y in 1000 flights, where n_y is the maximum lateral load factor measured during a turn; l_n represents the wheel base and l_m the track width. N_0 is the number of cumulative occurrences at $n_y = 0$; s represents a shape parameter specific to the aircraft being studied. Each aircraft therefore has its own factor for N_0 and s, that are derived from the study. The authors of [2] average the factors of all the aircraft to obtain a generic formula that can be used for any aircraft. Their initial assessments show that the taxi-in phase seems to generate larger load factors, but they point out that corrections need to be made to the taxi-in data, due to the fuel that is burned between the maximum ramp weight (MRW) and maximum landing weight (MLW) condition. Nonetheless, the taxi-in phase still seems to be more critical, even after such corrections are made. The generic formula to obtain the lateral load factor for the taxi-in phase then becomes

$$N = 2225.7e^{-l_n^{0.498}l_m n_y^2}. \tag{2}$$

This equation can be rearranged to obtain the lateral load factor as a function of the layout of the gears, and the probability of an occurrence of the obtained factor in 1000 flights. If we assume that the life of an aircraft is no more than 100,000 flights, then the value of N becomes 0.01. Figure 4(a) contains a contour map of the maximum lateral load factor that can be expected at least once in 100,000 flights, for different track width and wheel base combinations. Existing aircraft are overlaid onto the contour map, which shows that smaller aircraft experience higher lateral load factors than larger aircraft. This maximum value is still significantly lower than the 0.5g specified by the regulation. It can be seen that a maximum value of 0.28g is predicted for the A320, which has never been measured in the tests (see Figure 3(b)), and a value of between 0.16 and 0.17 is predicted for the A380.

The authors of [2] then insert the dimensions of the Boeing 737-400 into this equation, and calculate the probability of experiencing a 0.5g lateral load factor. This probability is used as a baseline for a comparison with other aircraft. Equation (2) is then used to obtain the maximum lateral expected load. Figure 4(b) shows the results from this study [2]. It is apparent from both parts of Figure 4 that the gear positioning and size of the aircraft have a major influence on the lateral load factor that can be achieved. This information can now be used by the FAA for future considerations pertaining to the regulation.

6

Table 1: Runway exit velocities obtained from the ICAO Aerodrome Design Manual [9].

Airplane Design Group	Exit Type	Radius (m)	V_n (m/s)
A	90°/135°	22.5	5.4
B		22.5	5.4
C		30.0	6.3
D		45.0	7.7
E		45.0	7.7
F		51.0	8.2
1,2	High-speed	275.0	18.9
3,4		500.0	25.5

3   Load Factors During Runway Exit Turns

The following subsection explores how the International Civil Aviation Organization (ICAO) determines the maximum exit velocity at a runway exit. Dynamic simulations of the A320 and A380 are then conducted at a typical runway exit in the subsections thereafter. The regulatory cases for lateral loading do not specify any dynamic behaviour during a turn. Rather, they only specify that the aircraft needs to be configured in such a way that a lateral side load factor of 0.5g is maintained. It is therefore implied that the dynamic loads do not exceed the steady-state loads. We aim to support this assumption in this section.

3.1   Runway Exit Design Velocities

The accelerations that are generated during a turn are highly dependent on the entry velocity into the turn. The International Civil Aviation Organization (ICAO) uses a steady-state lateral load factor (defined as the ratio of the lateral load at the CG to the weight of the aircraft) of 0.133 to determine the maximum design velocities that can be used at runway exits [9]. These velocities are obtained by using the formula for centripetal acceleration, inserting the load factor of 0.133, and then rewriting the formula in the form

$$V_n = 1.1422\sqrt{r_n},\tag{3}$$

where r_n represents the radius of the turn. Table 1 provides the design velocities that are obtained when this formula is used. The author has not been able to ascertain why the specific value of 0.133 was chosen for the load factor, but it does provide airport designers with a means of specifying runway exit velocities. The design rules stipulate that the operational velocities shall be below these values, and that they need to be determined empirically [9]. Each airline therefore stipulates its own rules with regards to exit velocities, which shall always be below the design values. Maximum operational velocities are typically 60% of the design velocity to ensure that all aircraft will exit runways in a safe operating region [9].

3.2   Load Factors for an A320

Figure 5 contains the steering angle, yaw rate, and lateral load factors, at different points of the aircraft, for an A320 that is conducting the prescribed turn. This is for the MRW and aft CG-position. The panels on the left in Figure 5 use time as the independent variable, while the panels on the right use the steering angle. Figure 5(a) therefore shows the evolution of the steering angle over time. Note that dynamic data from simulations are represented by solid curves, while steady-state values from continuation runs are represented by dashed curves. The dashed curve in Figure 5(a) represents the steering angle that is needed to maintain a radius of 51m at the nose gear, for the required velocity; it is obtained from continuation runs. Graphs with time as the independent variable show only the final steady-state value of steering angle that produces a turn radius of 51 m, while the dashed curves in the graphs that contain the steering angle as the independent variable represent the steady-state values for a set of steering angles. (This is equivalent to obtaining the graph by inserting a very slow ramp input, and then
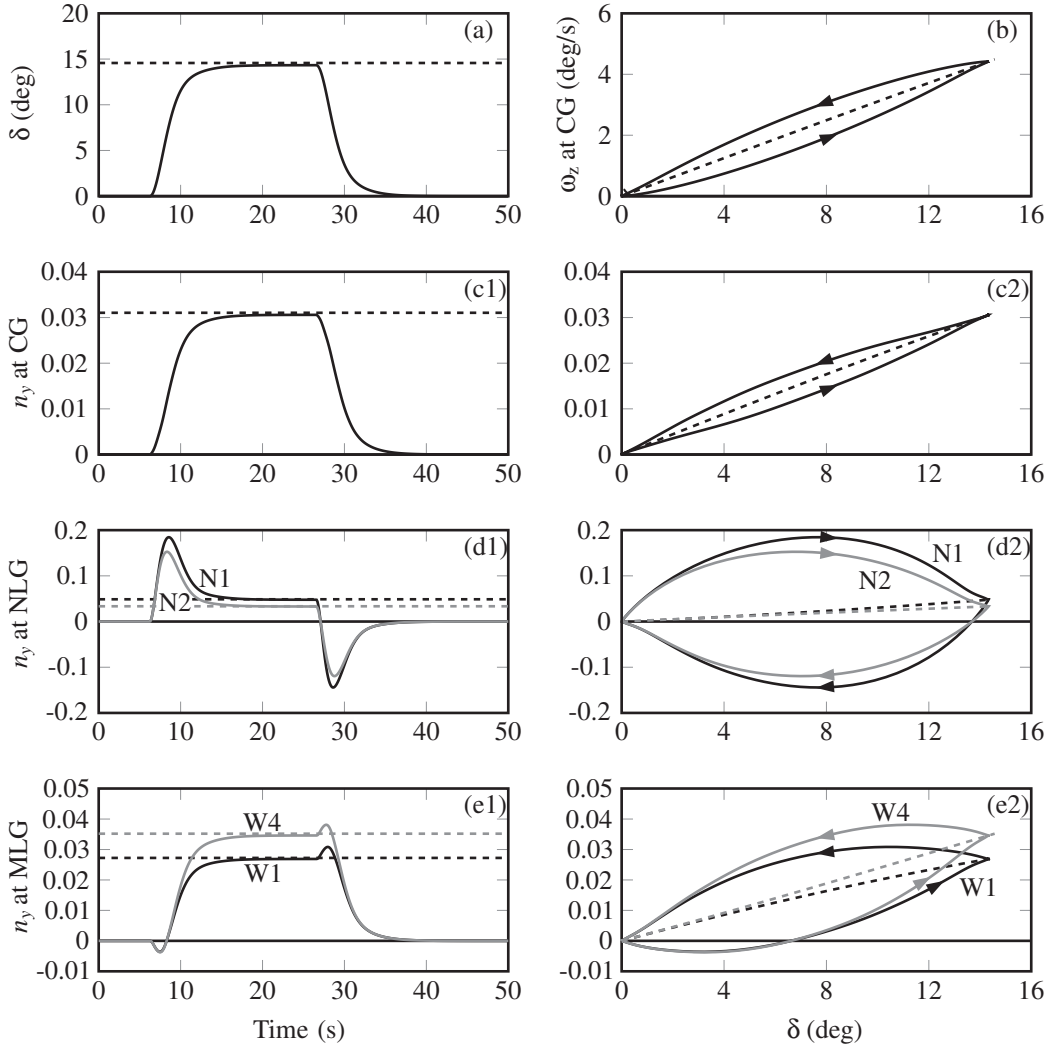
Figure 5: Evolution of the lateral forces of an A320 aircraft conducting a turn at a Group VI runway exit, while maintaining a nose gear velocity of 4 m/s. Panel (a) shows the evolution of the steering angle δ over time, where the dashed line indicates the steady-state steering angle that is obtained from the bifurcation method. Panel (b) shows the yaw rate ω_z around the CG as the steering angle is varied. The dashed line again depicts the steady-state values obtained from the bifurcation method. Panels (c1) and (c2) show the lateral load factor n_y at the CG-position. Panels (d1) and (d2) show the load factors for the outer (N1) and inner (N2) nose gear tyres. Panels (e1) and (e2) show the load factors for W1 and W4 .

recording the state values at each steering angle.) It can be seen that the steering angle reaches the steady-state steering angle during the turn, maintains this condition for a while, and then reduces to zero when the exit position from the turn is reached.

Figure 5(b) shows the yaw rate at the CG, and it illustrates that the yaw rate never exceeds the final steady-state value. Figures 5(c1) and (c2) depict the lateral load factor at the CG, used in the ground loads regulations. The graph shows that the lateral load factor converges to the final steady-state value without any overshoot. This result is unexpected, as there might be an overshoot that is larger than the final steady-state value. Overshoot usually occurs when step inputs are provided to the system, which is not the case in this analysis where an exponential input is used. Ramp inputs are also often used in simulations, where the nose gear is allowed to deviate from the centreline within certain margins [6]. The current approach of an exponential function that was developed in [10] for the steering angle is deemed to be the most realistic, as the pilot would act as a controller that maintains the nose gear close to the centreline.

Figures 5(d1) and (d2) show that the nose gear initially has to provide enough force to decelerate the aircraft along the fuselage axis, while accelerating the aircraft around the yaw-axis. The dashed curves once again represent the steady-state values when the nose gear follows a radius of 51m. Both components of the force are provided by the nose gear tyres. The aircraft will not be able to conduct the turn at the required radius if these forces cannot be provided. The force consequently
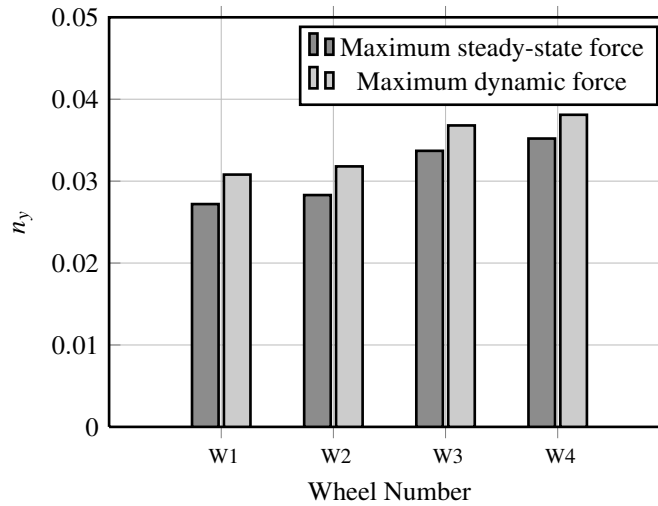
Figure 6: Dynamic and steady-state load factors on the main gear tyres for the A320 and $V_n = 4$ m/s. The nose gear maintains a radius of 51m.

builds up rapidly at the onset of the turn, and then reduces to the steady-state value. A significant overshoot is therefore present.

Figures 5(e1) and (e2) contain the lateral load factors for the outermost main gear tyre, W1, and innermost main gear tyre, W4. The main gear tyres initially resist the rotational motion at the onset of the turn, which can be seen from the negative values for the load factor. The forces then change direction and orientate to the general direction of the turn centre. In this case the forces build up towards the steady-state values. Note that the outer gear load factor is less than the inner gear load factor, even though the outer gear experiences higher vertical loads. This is due to a larger slip angle on the inner wheel (W4) when compared to the outer wheel (W1). An opposing force is also present when the aircraft tries to straighten out at the exit point of the turn.

The hysteresis in the graphs is indicative of nonlinearity in the system, which is mainly due to the tyre characteristics in these cases. The overshoot value for the main gear tyres do not exceed 10% of the steady-state value. It is possible to obtain the steady-state values directly from bifurcation diagrams, and then we can assume that the dynamic value will be approximately 10% larger than this value. This dynamic effect is ignored in the regulation for high-speed turns, but we will include this effect for the analysis of the A320. Figure 6 shows the maximum load factors that occur in the main gear tyres, associated with the peak values of the opposing force as the aircraft straightens out. Shown are the maximum dynamic, and steady-state values when the steering angle is maintained to follow a constant radius of 51 m. The steady-state values are not higher than 10% of the maximum dynamic values.

3.3   Load Factors for an A380

The next step is to look at an aircraft with more than two main gears. An A380 model at MRW and aft CG position is used for this purpose. A similar velocity and exit radius is used to that of the case for the A320, with a turn direction to the right. Figure 7 contains the steering angle, yaw rate, and lateral load factors at different points of the aircraft. In Figure 7(a) it can be seen that the steady-state steering angle is not reached for the case of a 90° exit, due to the larger wheel base; this is consistent with the steering angle results from Appendix C, where a steering angle of 32.72° is predicted, at the exit position, for the A380. This is in good agreement with Figure 7(a). It is interesting to note that the yaw-rate from the simulations in Figure 7(b) (solid line) is very close to the steady-state values that are obtained from continuation analysis (dashed line). The yaw rate at the CG-position does not reach the final steady-state value, and consequently it can be assumed that the steady-state value could be used as a maximum value for design purposes. Figures 7(c1) and (c2) show that the lateral load factor at the CG builds up towards a value that is close to the steady-state value, and contains no overshoot. The simulation results are once again close to the continuation results.

The largest difference in load factor occurs between the inner-most, and outer-most tyres, hence these tyres are used for the A380 comparisons that follow. The comparisons always progress from the nose gear tyres to the first row of the wing gear,
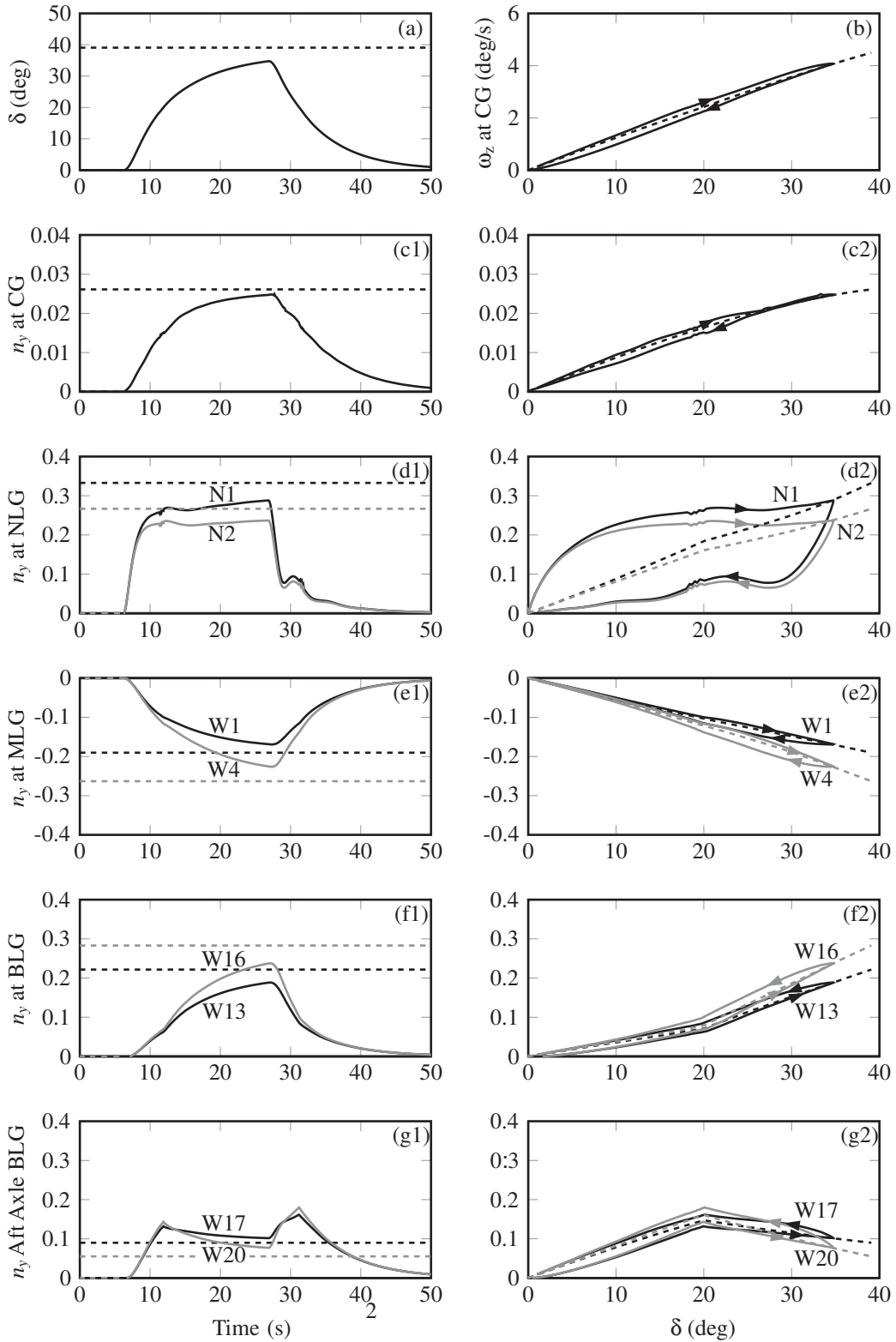
Figure 7: Evolution of the lateral forces of an A380 aircraft conducting a turn at a Group VI runway exit, where $V_n = 4$ m/s. The representation of the data in the different panels is as in Figure 5.
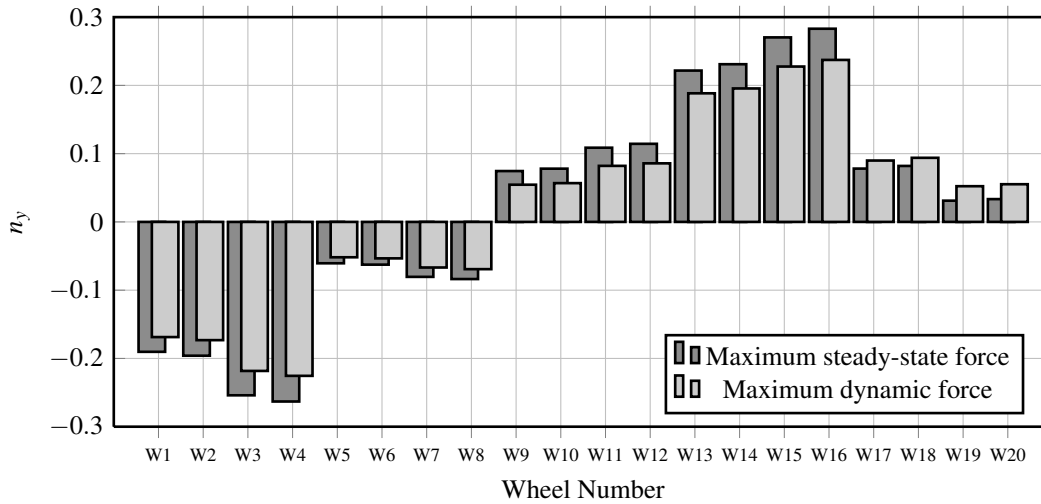
Figure 8: Dynamic and steady-state load factors on main gear tyres for the A380, when a radius of 51 m at the nose gear is maintained, for a nose gear velocity of 4 m/s.

then to the middle row of the body gear, and finally, the aft row of the body gear. The load factors in the other rows are significantly lower and are consequently not shown in the detailed comparisons. Figures 7(d1) and (d2) show that a large hysteresis loop exists in the nose gear tyres, N1 and N2, indicating nonlinear effects. Even though the dynamic values from simulations are significantly higher than the steady-state values, they still do not exceed the steady-state values when a turn radius of 51m is maintained.

Figures 7(e1) and (e2) depict the load factors for tyres W1 and W4. Figure 7(e1) shows that the final steady-state is not reached, while Figure 7(e2) shows that the dynamic values are close to the steady-state values during the turn. Figures 7(f1) and (f2) can be interpreted in a similar manner for W13 and W16. The tyres on the aft axle of the BLG, tyres W17 and W20, are shown in Figure 7(g1) and (g2), indicating similar load factors in both tyres. The dynamic loads are also larger than the final steady-state value if a radius of 51m is maintained. The kink in the curves indicate the point where the body gear steering switches on, indicating that significant load relief can be obtained by adding steering onto the aft axles of the BLGs. Figure 7(g2) shows that the dynamic values are not far from the steady-state values.

Figure 8 contains the steady-state load factors on all 20 of the main gear tyres when the nose gear maintains a radius of 51m, and also the maximum dynamic load factor values for a 90° exit. The steady-state values are more critical for most of the tyres, apart from the tyres on the aft axles of the BLGs, where the maximum dynamic values are approximately 10% higher for the aft axle wheels, when compared to the steady-state values. The overall steady-state loads on the BLGs are larger than the overall dynamic gear loads. The maximum tyre loads occur at the exit point from the turn (θ_{90}) for W1-W16. The maximum for W17-W20 occurs after θ_{90} when the aircraft straightens out. A similar pattern to that of the A320 emerges, where the inner tyres have a larger load factor compared to the outer tyres, even though the outer gears experience larger vertical loads.

We can therefore conclude that the dynamic load factors on the tyres of the A320 will be approximately 10% higher than the steady-state values. This is in contrast to the A380, where the steady-state values are more critical for most of the tyres, which is consistent with the interpretation of the lateral loads regulation. Towing loads cause significantly higher loads in the aft tyres of the BLGs, hence the dynamic effect on the aft axles of the BLGs are likely to be less important than for the towing case. One could therefore use the steady-state loads on an aircraft such as the A380 for design purposes, and add a correction to incorporate the dynamic effect for a smaller aircraft such as the A320. Continuation analysis provides these steady-state values.

4 Aircraft Loads from the Static Balance Equations

The high-speed turn regulation is interpreted by aircraft manufacturers to require the aircraft to conduct a turn by using nose wheel steering or differential power. A lateral acceleration of 0.5g and a vertical acceleration of 1g at the centre of gravity
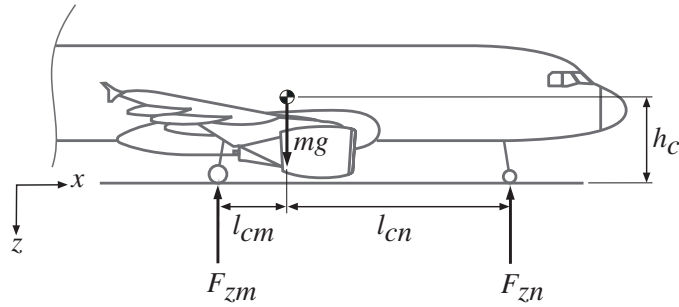
(a) Side view.
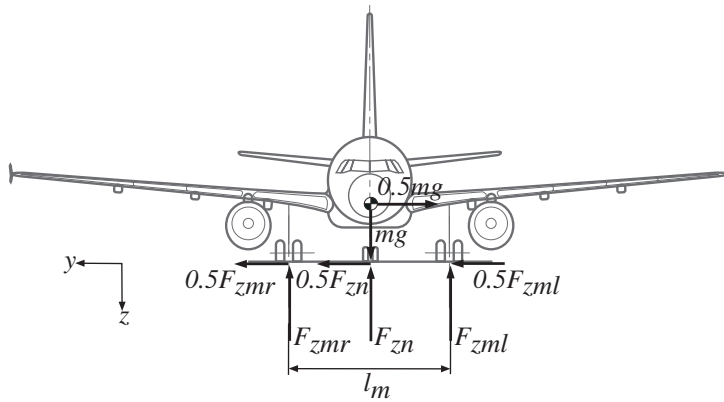
(b) Front view.

Figure 9: FAR25.495 lateral loads requirement depicted in free-body diagrams.

are considered. This section shows how the forces can be obtained from the static balance equations for an aircraft with three landing gears.

The aircraft is assumed to be in the level position, hence no roll angle is present. The lateral load at each gear is set to be half its vertical load. This scenario is depicted in Figure 9(b). The critical centres of gravity are chosen in accordance with the general requirement for ground loads (FAR-25.471), hence the range must be selected so that the maximum design loads are obtained in each landing gear element. Thus, both maximum forward and aft centre of gravity positions are investigated. Also, concerning the weight of the aircraft, FAR-25.489 states that unless otherwise prescribed, the landing gear and aeroplane structure must be investigated for the aeroplane at the MRW. No wing lift may be considered. The shock absorbers and tyres may be assumed to be in their static position. Finally, the runway conditions are assumed to be dry. This is significant, because patches of ice on the runway could reduce the friction on a specific gear, with a subsequent load transfer to other gears [11].

The loads can then be calculated by considering the static load balance of the aircraft. The vertical loads at the nose and main gear positions can be obtained by deriving the static balance equations from Figure 9(a). The thrust is ignored for these calculations (but is used later for the continuation analysis). The sum of the vertical forces at the tyres needs to equal the weight of the aircraft, while the moments around the CG also need to be in balance. The forces on the main gears also need to resist the rolling moment that is created by a lateral load factor n_y, and consequently the left-hand gear will see larger forces than the right-hand gear, for a turn to the right; as before, assume that a turn is made to the right, from the pilot's perspective. Figure 9(b) contains the forces and dimensions of interest for the lateral loading of the gears. The forces at each main gear can then be calculated as

12

Table 2: Vertical loads for A320 gears at maximum ramp weight and 0.5 lateral loading condition.

	CG-fwd	CG-aft
$l_{cn}(m)$	10.96	11.92
$l_{cm}(m)$	1.83	0.87
$F_{zn}(N)$	104019	49334
$F_{zml}(N)$	519772	547115
$F_{zmr}(N)$	101168	128511

$$
\begin{bmatrix} F_{zn} \\ F_{zml} \\ F_{zmr} \end{bmatrix} =
\begin{bmatrix}
\dfrac{l_{cm}}{l_{cn}+l_{cm}} & 0 \\[2ex]
\dfrac{l_{cn}}{l_{cn}+l_{cm}} & \dfrac{n_y h_c}{l_m} \\[2ex]
\dfrac{l_{cn}}{l_{cn}+l_{cm}} & -\dfrac{n_y h_c}{l_m}
\end{bmatrix}
\begin{bmatrix} mg \\ mg \end{bmatrix}.
\tag{4}
$$

Figure 10(a) depicts the vertical forces at the main gears for an A320 that are obtained from the static balance equations, in accordance with the regulation, as well as quasi-steady results obtained from a dynamic model. The main differences between the two methods of calculation is the absence of oleos, aerodynamics, and tyre properties, for the regulatory method. The steering angle in the model is set to $15°$, and then the velocity is ramped up gradually from 1 to 12 m/s. This provides forces that are close to the equilibrium values. An increase in the lateral load factor n_y at the CG, causes an increase of the vertical force on the outer gear, and a decrease of the force on the inner gear. The difference between the forces on the gears is larger for the method proposed by the regulation, due to the absence of aerodynamics. No equilibrium results were obtained in the model for $n_y > 0.27$, due to a loss of aircraft stability above these values [1, 4, 5]. This is discussed in the next section. The area to the right of the dashed lines indicate this unstable region. The regulation requires the most extreme positions for the CG, and therefore Table 2 contains the gear forces for the MRW of 73900 kg, at the extreme fore and aft CG positions.

There are two equations that can be used to calculate the three lateral wheel forces: a balance of the forces in the y-direction and the moments around the z-axis. The system in Figure 10(b) is underdetermined, and therefore a lateral load factor needs to be chosen for the wheels. The biggest assumption related to this regulation is that a lateral load factor of 0.5 is present at the tyres. We assume that the load factors at the gears are equivalent to the load factor at the CG, which is represented by the diagonal line, and is similar to the regulation. The quasi-steady results from the simulation show that the inner gear experiences a lateral load factor that is larger than the regulatory value, while the outer gear experiences a smaller value. If the values are extrapolated to the regulatory n_y value of 0.5 at the CG, the inner gear load factor would be larger than the 0.5 regulatory value for the gear. The inner gear factor is approximately 0.35 at the onset of limit cycles, where $n_y = 0.3$. The 0.5 regulatory factor is therefore adequate. Tyre properties are often altered to unrealistic values in simulations, to enable the generation of such large side load factors. This approach was not followed here.

Statically indeterminate gear arrangements cannot be solved by the previous calculation method, and therefore dynamic simulations are used for an aircraft such as the A380. Note that the original regulations were written in the days when tricycle arrangements were prevalent, hence the implementation of the regulation using static balance would have been adequate for most aircraft in operation. Simulations and continuation methods would fall under the banner of *rational* cases, which are discussed in the next section.

5   Continuation Analysis of the High-Speed Turn

A runway exit manoeuvre is essentially a transition from a straight line motion to a steady-state circular trajectory. Section 3.2 shows that the steering angle for the A320 converges to the steady-state value for a $90°$ exit, hence this is the maximum value that will be reached. The steering angle for the A380, on the other hand, does not reach the steady-state value at a $90°$ exit for a category VI airport, but does come close to this value when a $135°$ exit is used [10]. We can therefore conclude that the steady-state steering angle values would in fact be the maximum steering angle values that could be experienced during
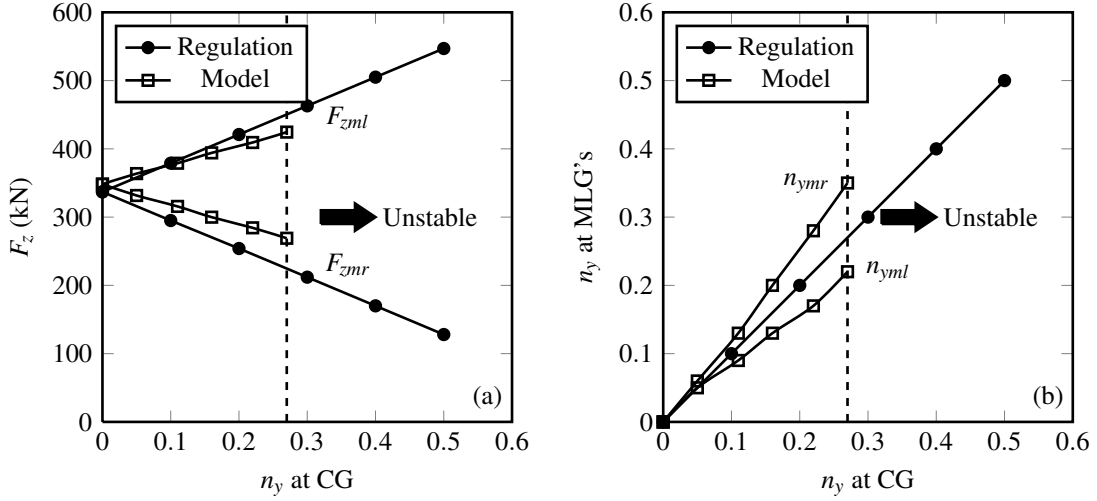
Figure 10: Comparison of the results from the static balance equations (in accordance with the regulation), and the results from a dynamic model of an A320. Panel (a) depicts the vertical loads on the main gears (F_{zml} = force on left gear and F_{zmr} = force on right gear), as the lateral load factor n_y is varied at the CG. Panel (b) depicts the lateral load factors at the gears. The MRW at the furthest aft CG position is used.

a turn. We will also assume that the steady-state lateral load factor at the CG position will be the maximum value. The steady-states can therefore be used to study the loads that can be experienced during ground manoeuvres. This is consistent with FAR 25.495.

Continuation analysis provides these steady-state values for different steering angle and thrust values, and hence provides a means in Sections 5.1 and 5.2 for the analysis of the high-speed turn. Previous ground dynamics studies of the A320 aircraft [1, 4] attributed fold and Hopf bifurcations to certain wheels that could not maintain the required force at the tyre-runway interface. The Hopf bifurcations could, for instance, be attributed to the loss of grip of the inner main gear tyres. A further study by Rankin et al. [6] showed that there was a strong correlation between the measured data from the FAA operational loads study and the results from dynamic simulations. The models that were used in this study did not contain oleos, while the axle widths on all the gears were set to zero. This was done to obtain significant improvements in the simulation times, while maintaining enough accuracy with regards to the stability characteristics. In the following sections we include all the effects that were omitted in the A320 model in References [5, 6], and also expand the analysis to the A380.

5.1 Load Factors for an A320

A similar approach is taken here as in the earlier studies [1, 4]. The initial steering angle is set to zero and then a velocity controller is used to find equilibrium states at this target velocity. The velocity controller is then switched off and the engine thrust is set to a constant value. The steering angle is then used as the continuation parameter, increasing to the maximum steering angle. The combination of all these different runs then allows for the construction of a bifurcation surface [4]. In this study we adhere to the configurations as stipulated by FAR 25.495, by considering the MRW condition at the extreme forward and aft CG positions.

Figure 11 shows the lateral load factor at the CG in a (δ, V_n)-projection of equilibria, constructed by bifurcation analysis. The top row represents the forward CG position, while the bottom row represents the aft CG position, at the MRW condition. The regulation states that the analysis needs to be done without aerodynamics and thrust. Cases that omit (left-hand panels) and include (right-hand panels) the aerodynamics are included here, to highlight the impact of the aerodynamics. Thrust is essential for the continuation analysis to work correctly, and is therefore included in all the analysis. The inclusion of thrust does in fact represent more severe loading conditions and would be more representative of reality [1]. The boundary between the shaded and white areas in each figure represent the Hopf bifurcations (labelled H) that were found in the original studies, indicating the onset of oscillatory behaviour [1, 3–5].

The contours labelled 30, 45, 51, 275 and 500, in Figure 11, indicate the steady-state radius in metres that the nose gear will follow, and they are related to the exit radii for different airport categories in Table 1. The line labelled 51 represents a
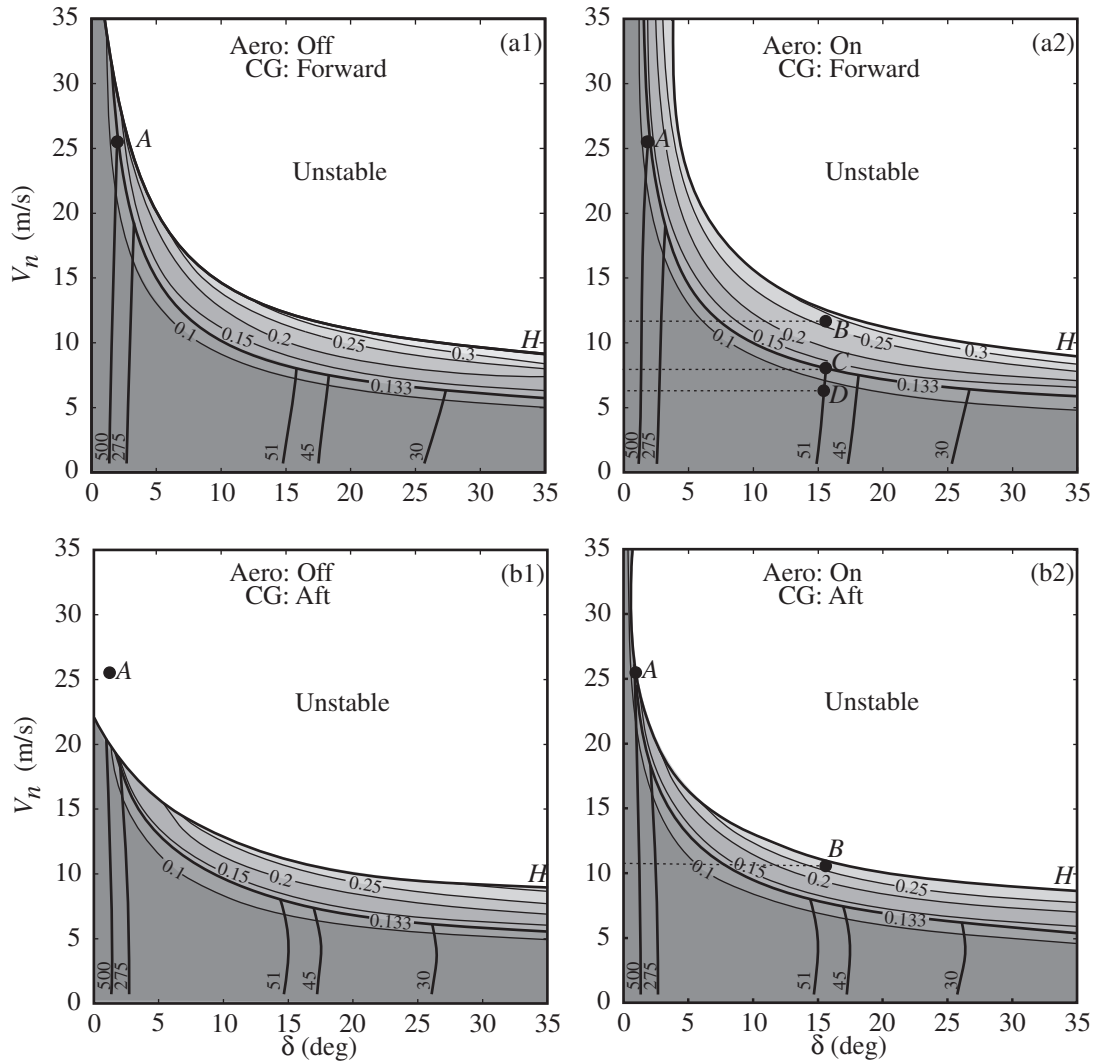
Figure 11: Lateral load factor contours at the CG for the A320 at the MRW, obtained from bifurcation analysis. The onset of instability is characterised by limit point and Hopf bifurcations. Panel (a1) is for forward CG position without aerodynamics; Panel (a2) is for the same configuration with aerodynamics included. Panel (b1) is with an aft CG position; panel (b2) is for the same configuration with aerodynamics included. The behaviour at points A, B, C and D are compared.

runway exit at a category VI airport; it shows that a steering angle of approximately $15°$ is needed to maintain a radius of 51m at the nose gear. The thick contour line between the 0.1 and 0.15 lines in the plots, represents the 0.133 ICAO lateral load condition, which is used for runway exit designs, as discussed in Section 3.1. The intersection points between the radii contours and the 0.133 contour provide the maximum steering angles and design exit velocities that can be used, according to the ICAO design rules. For example, point C in Figure 11(a2) indicates that a design runway exit velocity of approximately 8 m/s should be used for a $90°$ exit at a Category VI airport, which is consistent with the values in Table 1 that were derived from the ICAO method.

A comparison of Figure 11(a1) and (a2) shows that the aerodynamics has a stabilising effect at higher velocities: the unstable region is moved to the right. Both diagrams are very similar for velocities below 10 m/s. This added stability at higher speeds is not of any real benefit for this configuration due to the restrictions placed by the design velocities. Point A represents the 25.5 m/s design velocity for a high-speed exit as contained in Table 1. This intersection point shows that a maximum steering angle of approximately $2°$ would be required for a high-speed exit. In both cases point A falls within the stable region. The aft CG position is more critical, as is shown in Figures 11(b1) and (b2), as is evident from the movement of the Hopf-curve towards the lower left-hand corner. Panel (b1) is for no aerodynamics, and panel (b2) has this effect included. It is clear from panel (b1) that the 25.5 m/s exit velocity, as prescribed by the ICAO design rules, would be too high: point A falls within the unstable region. The aerodynamics once again plays a stabilising effect; panel (b2) shows that an aft CG configuration is
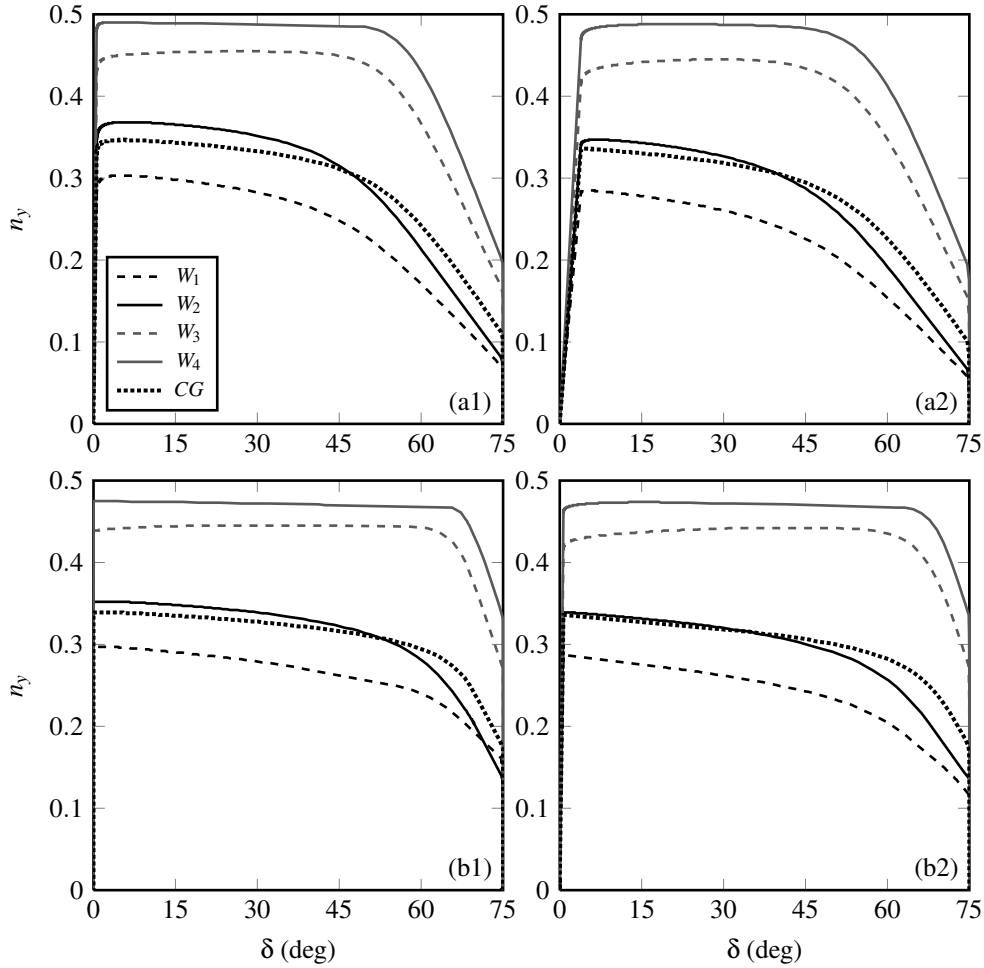
Figure 12: Maximum possible lateral load factors at the CG and wheel positions for the A320, MRW configuration. Panel (a1) is with a forward CG position, without aerodynamics. Panel (a2) if for the same configuration with aerodynamic effects included. Panel (b1) is for an aft CG position, while panel (b2) is for the same configuration, with aerodynamics included.

less stable than a forward CG configuration. This is to be expected.

FAR 25.495 aims to cover the extreme loading cases, hence another useful comparison is to plot the envelope of the maximum load factors at the CG and tyre positions. The data points from the bifurcation analysis can be represented as a cloud of individual points, where each point is associated with a steering angle, velocity and lateral load factor. All the data points are projected onto the (δ, n_y) plane. Maximum load factor envelopes for the CG and tyres are automatically generated by the Convex-Hull algorithms available in Matlab. Note that all the stable and unstable solutions are considered, giving the maximum possible values that can be generated. Figure 12 shows the maximum lateral load factors that can be achieved across the entire envelope for the MRW condition. The same configurations are considered as in Figure 11. Note that the load factors in the tyres are increased by 10% from the steady-state values to account for the overshoot that was observed in Section 3.

It is clear that the load factor at the CG of the A320 is not anywhere near the 0.5 value that is prescribed in the regulation. The inner-most tyres in the turn can experience lateral load factors that are close to the 0.5 value, but the tyres on the outside of the turn experience load factors that are significantly lower than the inside tyres, and slightly higher than the factors experienced at the CG, even though the vertical loads on the outside tyres are larger than the vertical loads on the inside tyres. This is due to smaller slip-angles on the outside gear. The velocity of the outside gear is larger than the inside gear, hence a smaller slip-angle is created. The forward CG position creates a gradual decline in the load factor as δ is increased, while the aft CG position seems to create a reasonably constant value, with a sudden drop after $60°$ of steering. The aerodynamics makes a significant difference at small steering angles and relates to the area around point A in Figure 11.

16

5.2 Load Factors for an A380

The A380 nose gear velocity drops very steeply towards lower velocities at small steering angles, when a constant thrust is used. Hence a large section of the envelope is not covered. This is not the case for the A320. The analysis technique for the A380 is therefore different to the approach taken for the A320. The velocity controller is not switched off during the continuation runs, and consequently the thrust is allowed to change as the steering angle is varied. A constant velocity is maintained at the nose gear, allowing for complete coverage of the envelope. This approach is only valid if no bifurcations are found. Bifurcations could indicate that some dominant engine modes are present if a velocity controller is used, which was indeed the case when the original studies were done for the A320 [1]. A lack of bifurcations for this case would mean that the results from a constant thrust or constant velocity approach would provide equivalent results. Note that the thrust was only applied to the inboard engines, which is similar to the way in which pilots taxi the aircraft. Figures 13(a1) to (b2) contain the results for the A380 lateral load factor at the CG, with similar MRW configurations as before. No bifurcations were found, hence no region of instability is present when compared to the dynamics of the A320. A lack of bifurcations indicate how remarkably stable this aircraft is when compared to a tricycle arrangement. The area below the 0.133 lateral load factor contour is again used to define the design envelope. This is the first time that a comprehensive map of the lateral load factor has been constructed for such a large aircraft, where such a wide range of steering angles and velocities are covered.

The areas below the 0.133 contour in panels (a1) to (b2) are almost equivalent, showing that the CG position does not have any significant influence on the loads within the design envelope. The left-hand panels (a1 and b1) have no aerodynamics included. The inclusion of aerodynamics in the right-hand panels (a2 and b2) shows that the aerodynamics causes a significant reduction in the overall loads that can be achieved. The aerodynamics reduces the maximum load factor by approximately 21% to 0.26 for the forward CG position, and by approximately 34% to 0.23 for the aft CG position, at the MRW. This may seem significant when compared to the A320, but note that these differences occur again at high-speed outside of the design envelope.

The most significant areas in the graphs in Figure 13 are in the bottom right hand corner of each panel, which corresponds to 90° and 135° exit manoeuvres at Category VI runway exits. The lines marked 51 are therefore of relevance. In panels (a2) and (b2) the effect of the aerodynamics pushes the 51 line closer to the 0.133 contour (the design envelope), when compared to panels (a1) and (b1). This is surprising when one considers that the velocity is only approximately 8 m/s. This may seem like a low velocity, but the huge aerodynamic surfaces of the A380 cause significant forces, even at such low velocities. In this particular case, this is due to the vertical tailplane. In Figure 13(b2) it can be seen that the combination of the aft CG position and the aerodynamics causes interesting ground handling problems at velocities in the region of 8 m/s. The 51 m curve transitions from an almost vertical gradient at low velocities to an almost horizontal gradient at approximately 8 m/s. A smaller force is present at the NLG due to the aft CG position, hence the NLG tyres saturate earlier when compared to the forward CG position. This means that no additional force can be generated from the NLG tyres, which are operating at the limit of their performance [1, 4]. The implication is that the aircraft cannot conduct a tighter turn than 51m when a velocity of 8 m/s is maintained at the NLG. The recommended velocity of 4 m/s (8 knots) ensures that these types of turns can be conducted safely for all configurations.

The curves representing the 275 m and 500 m radius high-speed exits show interesting behaviour in regions that the aircraft will never venture into. As an example, let us examine Figure 13(b2). If the aircraft maintains a velocity of 25 m/s at the NLG, and the steering angle is gradually increased, the radius of the nose gear trajectory will decrease, until the steering angle reaches a value of approximately 11°. The trajectory of the nose gear will maintain an almost constant radius between 11° and 20° degrees. This radius will increase after 20° as the steering angle is increased. This is due to the nonlinear nature of the tyre, and it can be seen in all the panels; the maximum side force available from the tyres is limited, as indicated by the white region in panels (b1) and (b2). The nose gear tyres in panels (a1) and (a2) are close to saturation in a similar region, and are operating at approximately 95% of the total available force. The aircraft is stable within the design envelope at high-speed exits. One could argue that the close spacing of the contours at low steering angles and high velocities make it easy to generate significant lateral load factors at high-speed exits. However, a pilot would not oversteer easily at such exits due to large radii of the turns, and also due to envelope protection laws in the flight control system.

The lateral loads requirement assumes that the forces on the gears act towards the turn centre, hence all the forces act in the same direction. This is however not the case for the A380. Figure 14 contains the lateral load factor contours in the (δ, V_n)-plane. Panels (a1) and (a2) contain the load factors on the WLGs, and (b1) and (b2) the BLGs. The negative contours at low velocities in panels (a1) and (a2) indicate that the gear forces on the WLGs act in an opposite direction to that of the BLGs, and change direction (to act in the same direction as the BLGs) at nose gear velocities above 10 m/s. This effect can be mainly attributed to the geometric layout of the landing gears, and to a lesser extent the tyre properties. The slip-
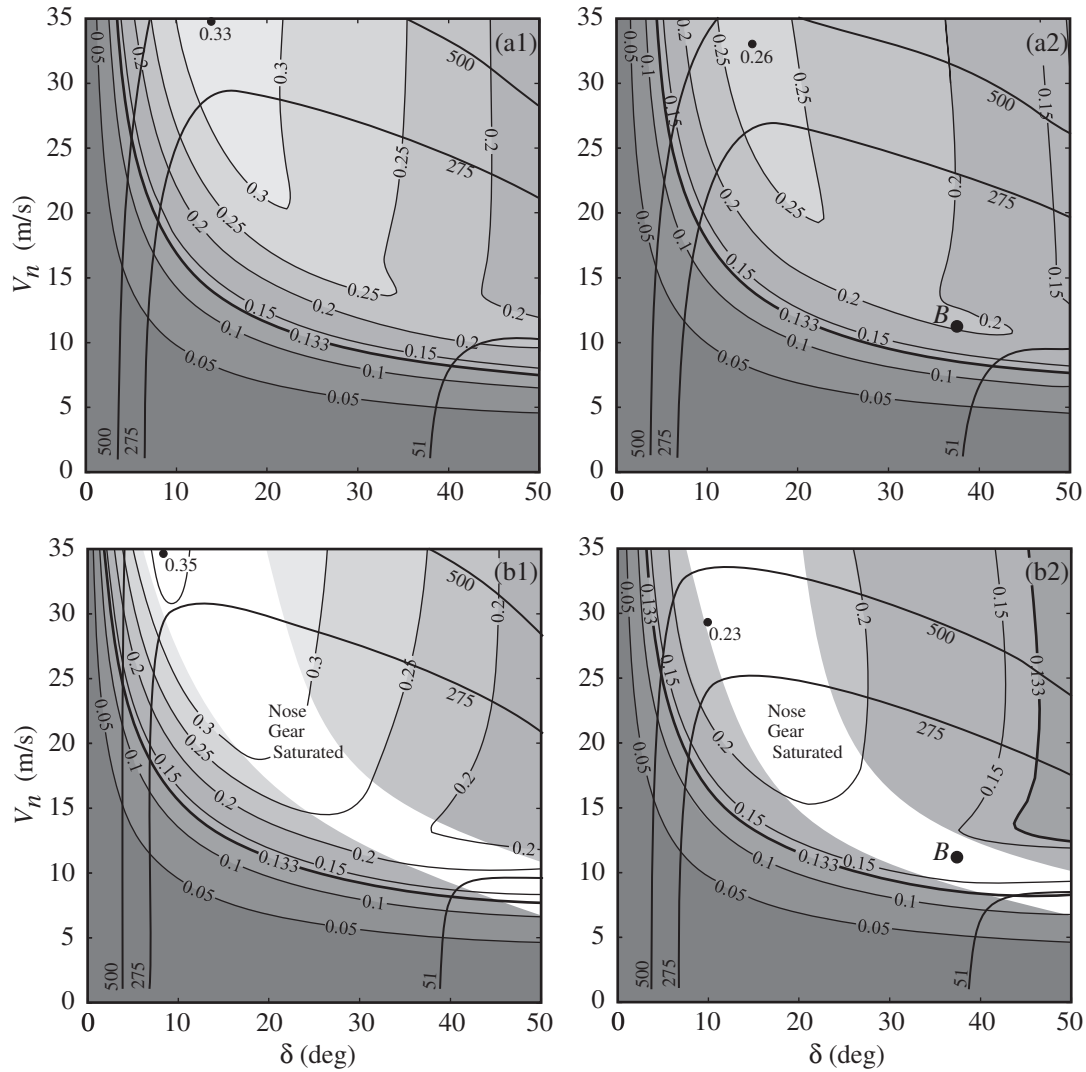
Figure 13: Lateral load factors at the CG obtained from continuation analysis for the A380 in the MRW configuration. Panel (a1) is for a forward CG position without aerodynamics; panel (a2) if for the same configuration with aerodynamics included. Panel (b1) is for an aft CG position; panel (b2) is for the same configuration with aerodynamics included.

angle is positive at low velocities, creating negative lateral loads. An increase in the velocity decreases the slip-angles, and consequently the lateral loads decrease. This can be observed in the reduction of the magnitude of the negative contours, in the bottom right-hand corner of Figures 14(a1) and (a2). Velocities above 10 m/s create negative slip-angles, with positive loads on the WLGs. If we start in the lower left-hand corner of panels (b1) and (b2), an increase in velocity and steering angle would lead to an increase in lateral load. The opposite is true in the top right-hand corners of these panels. The effect of the steering system on the aft axles of the BLGs is not readily apparent from these graphs; it will be more pronounced in the next section, when the focus shifts to the tyres.

5.3 Individual Tyre Loads for an A380

The extensive amounts of information provided from bifurcation methods allows one to present the results in a different way. Figure 15 is an example. It shows a map of the tyre that is carrying the largest lateral load as the steering angle and velocity is varied. A complex pattern emerges for the A380. For example, for $V_n = 5$ m/s the maximum load switches between five different tyres. The inner tyre on the aft axle of the body gear, W20, initially generates the highest load. The body wheel steering system engages at $20°$ and a consequent shift occurs to W18, then W4, progressing on to W16, and finally to W15. This type of diagram allows engineers to gain a much improved understanding of the loading in the system, and it is a pertinent example of how complex the behaviour of such a large aircraft can be.
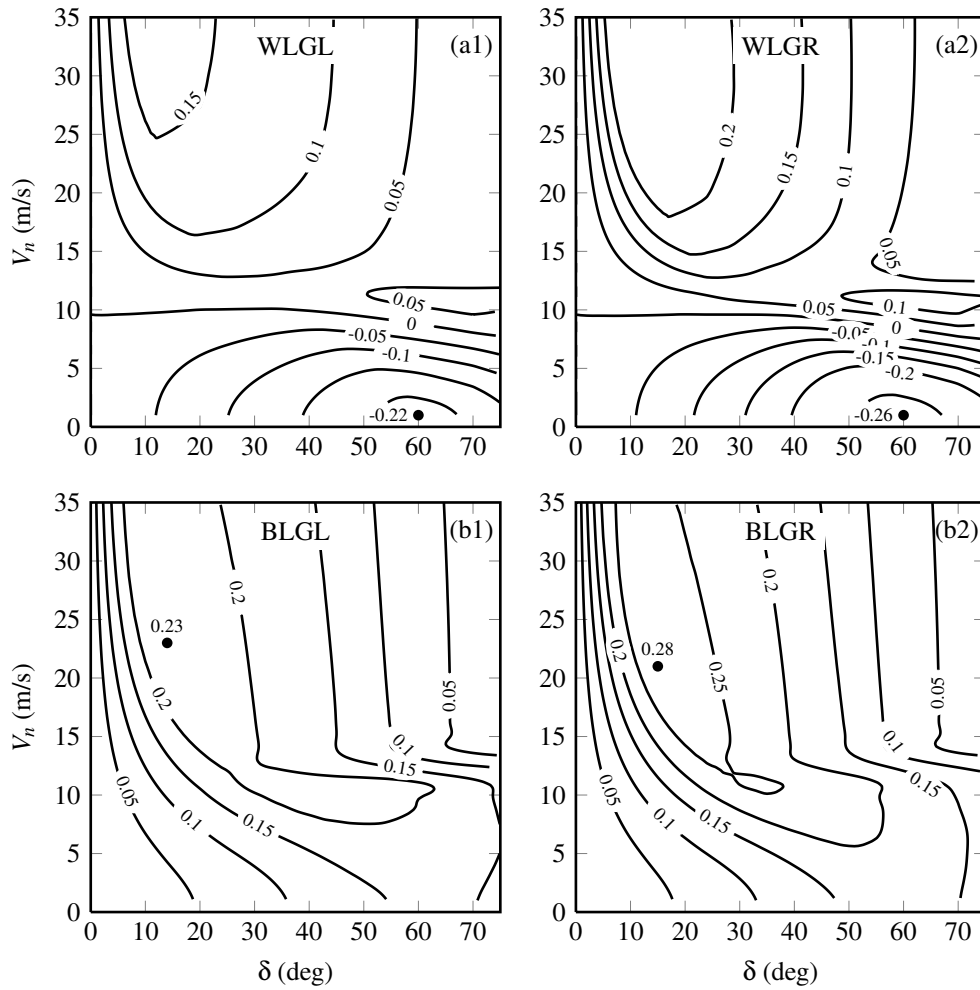
18

Figure 14: Lateral load factor on each gear for the MRW aft CG configuration of an A380.
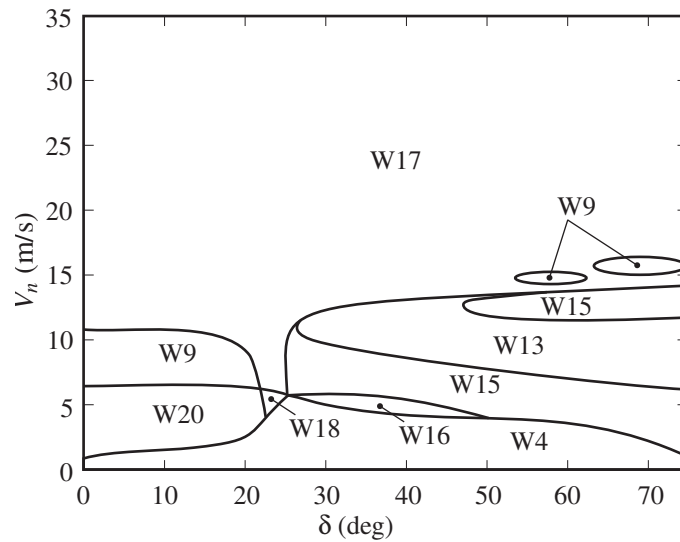

Figure 15: Map of tyres of the A380 that carry the highest load as the steering angle and velocity are varied. The number in each area indicates the tyre with the highest lateral load. The MRW condition with an aft CG position is used.
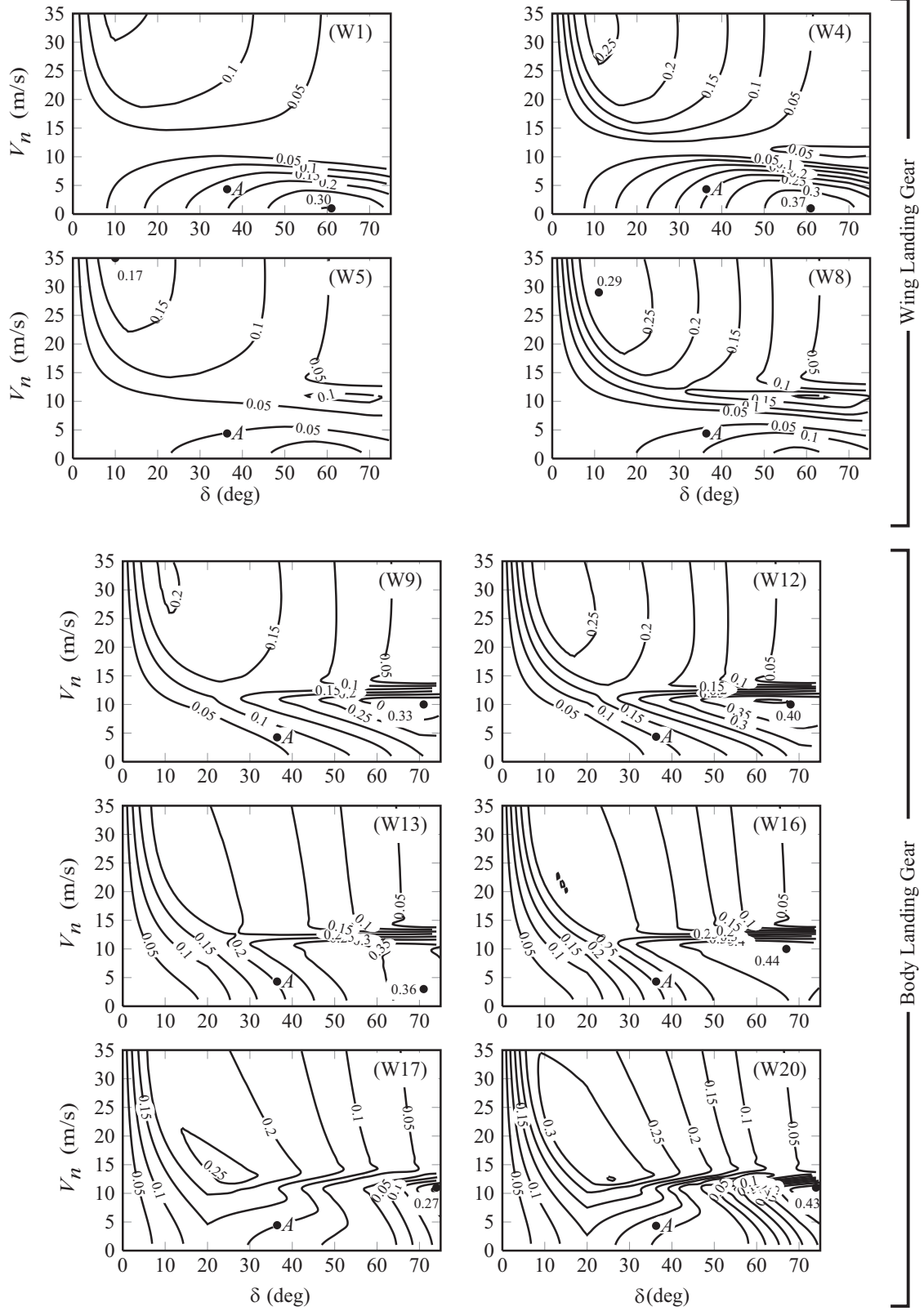
Figure 16: Contour maps of the absolute steady-state lateral load factor, for the outer-most and inner-most tyres, during a turn. The panel numbers depict the wheel numbering convention from Figure 1.

The last piece of the puzzle is to consider the lateral load factor on individual tyres. Only the inner-most (W4,W8,W12,W16,W20) and outer-most (W1,W5,W9,W13,W17) tyres are considered in Figure 16. The absolute values are shown. We can observe that the inner tyres experience a higher load factor than the outer tyres. This is due lower slip-angles on the outer tyres. The maximum forces at the tyres can easily be obtained for a Group VI runway exit. A steering angle of approximately $37°$ represents the steady-state steering angle for a Group VI exit [10]. If the exit velocity is restricted to 4 m/s, the coordinates $(\delta, V_n) = (37, 4)$, would indicate the point where the maximum tyre forces can be expected for this type of exit. These co-ordinates are represented by the points labelled *A* in Figure 16. If we then look at the load factors at these points, it can be seen that the first row of tyres on the wing gear, and the middle row of tyres on the body gear, carry the highest loads. This would be the most likely scenario in terms of operational velocities and steering angles. An unrealistic scenario would be at approximately 11 m/s, where the second row of tyres on the wing gears carry the highest load factors, and most of the other tyres appear to have low load factors.

The body wheel steering does not seem to have much of an effect on the load factors at the wing gear tyres. There is however a significant effect on the body gear tyres, as can be observed by the patterns in the contours around a $20°$ steering angle. The body wheel steering does provide significant load alleviation in the body gear tyres, W17 and W20, which was also apparent in the simulation results in Section 3. The difference between the load factors on the inner and outer gears are less than for the A320. Most of the wheels are not anywhere near the 0.5 factor stipulated by the FAA regulation, apart from the inner wheels of the body gear. We see, therefore, that continuation methods allow for a full classification of the load factors within the tyres. The exact conditions where these maximum values occur can be identified very efficiently.

6 Relating the Continuation Results to the FAA Study

The final step is to relate the statistics from the FAA study with the results obtained in the previous sections. Only the more realistic cases with aerodynamics are considered here. Figure 17 compares the envelope that is obtained from the continuation analysis, with the A320 data from the FAA study in [12]. The lateral load factors were recorded over 10066 flights, where approximately half of the runway exit angles were below $60°$, a quarter were between $60 - 120°$, and a quarter were larger than $120°$. The outliers at zero velocity are likely to be due to measurement errors, or could possibly be attributed to gusts on the apron; they can be safely ignored. All the data of significance therefore lies within the envelope. Runway exits smaller than $60°$ seem to generate the highest loads; however, there are significantly more data points for this type of exit. Similar maximum values may arise when more data points are added for the other exits. It is interesting to note that [12] could not show any statistical correlation between the exit velocity and the lateral load factor that is generated. The large void at higher velocities shows that the analysis method covers cases that would not occur operationally. The lower maximum load factor of 0.33, when compared to the 0.5 value from the regulation, indicates that the method is less restrictive than the regulation, yet seems to be adequate to cover the operational cases.

The results can also be used to determine the maximum likely lateral load factor in operation. It can be seen from Figure 4(a) that a lateral load factor of approximately 0.28 can be expected at least once in a lifetime for an A320, and a load factor of 0.17 for an A380. The fact that the exit velocity and exit type seems to be statistically insignificant, makes the choice of an operating point difficult. We therefore choose a point that is representative. Point *B* in Figures 11(a2) and (b2) would correspond to a load factor of approximately 0.28 at a runway exit for a Category VI airport. We will therefore assume that 12 m/s is an extreme exit velocity at a $90°$ exit for the A320 and A380, and also that all $90°$ runway exit manoeuvres are conducted below this velocity.

The lateral load factor of 0.28 at point *B* in Figure 11(a2) can be reached in one of two ways. The first scenario is where the entry velocity into the turn is approximately 12 m/s, while the pilot adjusts the thrust through the turn to try and maintain the velocity. The second scenario is that the pilot enters the turn at 6 m/s (point *D*), then increases the thrust to try and maintain the velocity, over-correcting the thrust above the required value and accelerating through the turn up to point *B*. This scenario seems more plausible if it is assumed that pilots adhere to the rules.

If we assume a maximum nose gear velocity of 12 m/s for the A380 in a turn, and then determine the maximum load factor in the region below 12 m/s, the maximum condition is then indicated by point *B* in Figures 13(a2) and (b2). Even when we ignore the fact that the aircraft would be unable to maintain a radius of 51 m at this velocity, we can see that it would be impossible to obtain a load factor of more than 0.2 for the forward CG configuration in panel (a2), and 0.17 for the aft CG position in panel (b2). Note that the contours are also spaced further apart from each other for the case of the A380. Hence, a change in thrust would not have as much significance when compared to the closely spaced contours for the A320. The closely spaced contours of the A320 mean that it is easier to obtain higher load values close to the unstable area. The value
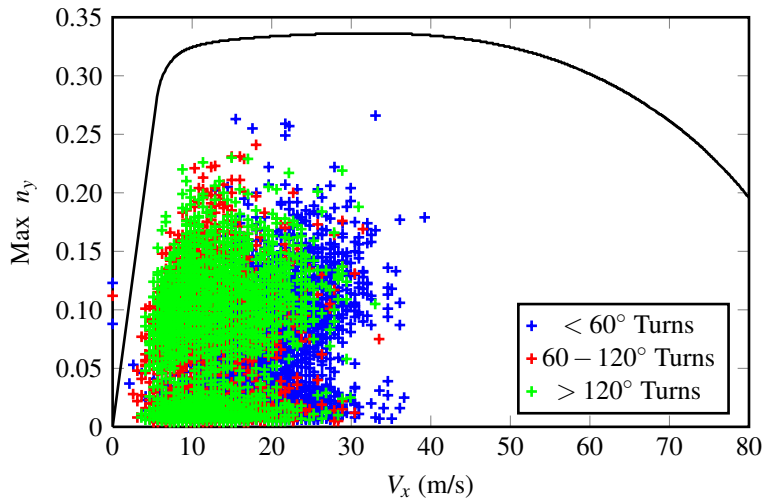
Figure 17: Comparison of maximum lateral load factor envelope (solid line) obtained from continuation analysis, and data points obtained from FAA study [12]. The MRW aft CG configuration is used for the envelope calculations.

of 0.2 for the forward CG is 10% higher than the expected 0.17 value, while the aft CG correlates exactly with the initial predictions in Figure 4(a).

7 Conclusions

An operational loads study by the FAA showed that large aircraft with statically indeterminate gear arrangements, such as the A380, do not generate the high loads that are stipulated in the requirements for a high-speed turn. We therefore compared the loads that can be generated by a relatively small (A320) and large aircraft (A380) to see how the results compare with the findings of the FAA. Static equilibrium equations were used to calculate the vertical forces on the gears of the A320. We showed that assumptions were needed with regards to the lateral load factor on each gear, due to the underdetermined nature of these equations in the lateral direction. The FAA therefore assume a 0.5 load factor, and it is this factor that gives rise to the conservative nature of the regulation. Simulations of the A320 showed that the inner gear experiences a higher lateral load factor than the outer gear. Extrapolation showed that a higher lateral load factor than the 0.5 value from the regulation would be experienced at the inner gear, if it were feasible for the aircraft to generate 0.5g at the CG position. This is however not possible, as the aircraft loses lateral stability at approximately 0.27g. Static balance equations cannot be used for the analysis of the gear loads of the A380, due to the underdetermined nature of the equations in all directions. Continuation methods were therefore used to obtain the lateral load values for this aircraft type.

Contour maps of the lateral load factor were constructed as a function of the steering angle and velocity at the nose gear of the A320, for the MRW condition. Different CG positions and aerodynamic configurations were considered. The aerodynamics did not have a significant effect on the maximum load that could be generated, as the maximum condition tends to occur at relatively low velocities (below 10 m/s). The results confirmed the findings from the simulations and showed that the load factors on the outer tyres are significantly lower than the load factors on the inner tyres. This is due to the larger velocity of the outer tyres, and consequent lower slip-angles. The results were also used to show how the maximum lateral load factors from the FAA study might have occurred. Similar maps were constructed for the A380 at the MRW condition with different aerodynamic configurations; they showed far less interesting dynamics from the dynamical systems perspective.

The demonstrated stability of the A380 during ground manoeuvres is of course desirable from an engineering perspective. We showed that the aerodynamics plays a significant role in the alleviation of the lateral loads. It was shown that the aerodynamics causes the nose landing gear tyres to saturate, moving the effective steering envelope closer to the design envelope specified by ICAO. The aerodynamics also causes a significant reduction in the lateral load factor, when compared to the case without aerodynamics. The analysis also showed that, at low velocities, the lateral loads on the WLGs act in an opposite direction to that of the BLGs. This is contrary to the assumption made in the regulation, where it is assumed that the forces on the gears act towards the turn centre. The forces on the WLGs reduce with an increase in velocity and eventually act in the same direction as the BLGs. Continuation analysis also allows for the construction of complex maps

22

that show how the tyre forces evolve as the steering angle and velocity is varied. This is very useful when parameter studies are conducted. We therefore showed that an aircraft such as the A380 would not exceed a lateral load factor of 0.26 across the entire envelope – almost half the value of the stipulated regulation.

The last section defined a typical operating envelope for the A380, and it compared the results from the analysis with the original FAA studies. These results show that a maximum lateral load factor between 0.17 and 0.2 would be experienced over the life time of the aircraft, and this correlates very well with the results from the FAA study. This provides additional evidence that a lateral load factor of 0.5 cannot be reached for such a large aircraft.

References

[1] Coetzee, E., 2006. "Nonlinear Aircraft Ground Dynamics". Master's thesis, University of Bristol.

[2] Tipps, D., Rustenburg, J., Skinn, D., and DeFiore, T., 2003. Side Load Factor Statistics From Commercial Aircraft Ground Operations. Tech. Rep. UDR-TR 2002-00119, Federal Aviation Administration, U.S. Department of Transportation, Federal Aviation Administration, Office of Aviation Research, Washington, DC 20591, January.

[3] Coetzee, E., Krauskopf, B., and Lowenberg, M., 2010. "Application of Bifurcation Methods to the Prediction of Low-Speed Aircraft Ground Performance". *Journal of Aircraft,* **47**(0021-8669), pp. 1248–1255.

[4] Rankin, J., Coetzee, E., Krauskopf, B., and Lowenberg, M., 2009. "Bifurcation and Stability Analysis of Aircraft Turning on the Ground". *AIAA Journal of Guidance, Control, and Dynamics,* **32**(2), March, pp. 500–511.

[5] Rankin, J., Krauskopf, B., Lowenberg, M., and Coetzee, E., 2010. "Operational Parameter Study of Aircraft Dynamics on the Ground". *ASME Journal of Computational and Nonlinear Dynamics*(CND-09-1022).

[6] Rankin, J., Krauskopf, B., Lowenberg, M., and Coetzee, E., 2010. "Nonlinear Analysis of Lateral Loading During Taxiway Turns". *Accepted for publication - Journal of Aircraft*.

[7] Anon. Part 25. Tech. rep., Federal Aviation Administration, year = 1980, journal = Airworthiness Standards: Transport Category Airplanes. FAR, pages = 252–439.

[8] Wright, J., and Cooper, J., 2007. *Introduction to Aircraft Aeroelasticity and Loads*. Wiley.

[9] International Civil Aviation Organization, 2005. Aerodrome Design Manual (Doc 9157) Part 2: Taxiways, Aprons and Holding Bays. Tech. Rep. 9157,AN/901, International Civil Aviation Organization.

[10] Coetzee, E., Krauskopf, B., and Lowenberg, M., 2010. "Analysis of Medium-Speed Runway Exit Maneuvers". In AIAA Modelling and Simulation Technologies Conference, AIAA, ed., no. AIAA-2010-7616, American Institute of Aeronautics and Astronautics, AIAA.

[11] Finn, E., Gleich, R., Green, K., Saccarelli, R., and Szot, M., 2007. Investigation of Limit Design Lateral Ground Maneuver Load Conditions. Tech. Rep. DOT/FAA/AR-07/38, Federal Aviation Administration, June.

[12] Rustenburg, J. W., Skinn, D. A., and Tipps, D. O., 2002. Statistical Loads Data for the Airbus A320 Aircraft in Commercial Operations. Tech. Rep. DOT/FAA/AR-02/35, Federal Aviation Administration, April.